Düzce University Journal of Science and Technology
Düzce Üniversitesi Bilim ve Teknoloji Dergisi

14 (2), 2026, 461-476.
https://doi.org/10.29130/dubited.1744260

e-ISSN: 2148-2446
https://dergipark.org.tr/en/pub/dubited

Research Article

Patch Antenna Design for Smart Grid Data Transmission at WiMAX and ZigBee Bands

Barış Gürcan Hakanoğlu[1*], Mehmet Güçyetmez[2], İbrahim Burak Koç[3], Semih Korkmaz[4]

[1] Atılım University, Engineering Faculty, Department of Electrical-Electronics Engineering, Ankara, Türkiye.
ror.org/04pd3v454

[2] Sivas University of Science and Technology, Engineering and Natural Science Faculty, Dept. of Electrical-Electronics Engineering, Sivas, Türkiye.
ror.org/05s32j989

[3] Ankara University, Institute of Accelerating Technologies, Ankara, Türkiye.
ror.org/01wntqw50

[4] Bandırma Onyedi Eylül University, Engineering and Natural Science Faculty, Dept. of Electrical-Electronics Engineering, Balıkesir, Türkiye.
ror.org/02mtr7g38

*Corresponding author:
baris.hakanoglu@atilim.edu.tr

Received: 17.07.2025
Revision: 06.02.2026
Accepted: 11.02.2026
Online: 19.04.2026

Abstract: In this study, new patch antenna designs operating in the WiMAX and ZigBee bands are proposed for smart grid data communication. The same design procedure has been repeated for different dielectric materials such as FR4, RO3203, RT6006, used in the patch antenna structure. This way, it has been determined which material exhibits more efficient propagation characteristics at the target frequency bands. Thanks to the proposed rectangular slots on the antenna, improvements have been achieved both in return losses and in operational bandwidths. The slot dimensions have been chosen as specific multiples of the wavelength for each material, enabling the generalization of the design procedure. Moreover, the width and length of the first slot were taken as $\lambda/50$ and $\lambda/20$, respectively, which resulted in an increase in the antenna's bandwidth. Then, the dimensions of the second rectangular slot were defined relative to the first slot, with its width set to half of the first slot's width and its length set to four times the first slot's length, yielding a further enhancement in the bandwidth. The antennas designed in the simulation environment have been fabricated using the printed circuit board (PCB) etching method. It has been demonstrated that the antennas measured with a vector network analyzer operate at the designed frequency as transmitter and receiver with the help of a signal generator and a spectrum analyzer.

Keywords: *Smart grid, Data communication, WiMAX, ZigBee, Patch antenna*

I. INTRODUCTION

Smart grids are a modern evolution of traditional electric power grids that adopt the latest information and communication technologies to create a more efficient, reliable, sustainable and cost-competitive energy infrastructure (Belu, 2013). High-tech grids aim to optimize all processes from energy production to consumption, facilitating the two-way flow of energy and information (Kabeyi & Olanrewaju, 2023), as well as increasing the use of renewable energy sources (Kataray et al., 2023). In this way, they encourage consumer participation and provide a more stable infrastructure in the event of a power grid failure (Colak et al., 2020). However, the smooth operation of such dynamic and complex systems largely depends on the ability to achieve continuous and high-performance data communication between various devices, and data communication capability is a limiting factor for smart grids (Abrahamsen et al., 2021).

In a smart grid, the wireless communication infrastructure that supports data transfer, especially the antenna design, plays an important role in the overall success of the system. Smart grids, which span large geographical areas, contain a large number of sensors, meters and control devices, and efficient communication between these devices and central control systems is possible thanks to properly designed antennas. Therefore, poor antenna performance can lead to signal attenuation, interference in communication and data loss, and can significantly reduce the efficiency of monitoring and controlling the grid. Therefore, antenna selection and design are critical priorities in the planning and implementation phases of smart grid projects (Sendin et al., 2021).

Another important consideration during antenna design is meeting the data rate and bandwidth requirements of the smart grid. These networks transmit data of various types and sizes, from energy usage readings to fault data, control signals, and even video streams. High data rates and extensive bandwidth utilization are facilitated by properly designed antennas that maximize the capabilities of the communication technologies used (Kishore & Senapati, 2022). Poorly performing antennas can limit data transfer rates and potentially hinder the efficiency of real-time monitoring and control applications. A stable and robust communication infrastructure, provided by effective antenna design, meets one of the most important requirements of smart grids by ensuring timely transmission of essential control commands and fast and accurate responses to grid events.

Energy efficiency and cost-effectiveness also play an important role in antenna design for smart grid data exchange. Properly designed antennas enable effective communication even under suboptimal power conditions, optimize device energy efficiency, and thus extend battery life (Pandiyan et al., 2024). Additionally, optimal antenna selection and

This is an open access paper distributed under the terms and conditions of the Creative Commons Attribution-NonCommercial 4.0 International License.

placement can reduce the need for unnecessary hardware duplication, such as repeaters and amplifiers, and reduce overall system costs by reducing maintenance requirements and ensuring longevity. Another contribution of an efficient antenna design to smart grids is that, due to the future growth and scalability goals of smart grids, an effective antenna design approach enables the creation of a scalable and adaptable communication infrastructure (Abdul Salam et al., 2024). From a manufacturing technology perspective, three-dimensional (3D) antenna structures have recently become an important research topic. These antennas' complex geometries can be fabricated with high precision using advanced additive manufacturing techniques, thereby improving their electromagnetic performance. In addition, due to advantages such as low power consumption, steerable radiation characteristics, and compact form factor, 3D antenna designs have been proposed in the literature as a potential solution for improving bandwidth and IoT applications utilizing Wi-Fi backscatter communication (Onay & Dokmetas, 2025; Dokmetas et al., 2024).

In this study, new patch antenna designs to meet the data communication needs in smart grids are examined for different dielectric materials and WiMAX and ZigBee patch antenna design is performed. A total of six antennas, three for each frequency band, are designed and analysed. The study is especially important in terms of determining which dielectric material should be preferred in the frequency region of smart grid data transmission.

II. DESIGN

In this section, the materials, instruments, and devices used should be presented clearly and in detail. Experimental setups, preparation steps, and analysis methods should be described in a way that ensures the reproduce reproducibility of the study. The specifications of the devices, equipment, or software used should be stated whenever possible. Standard solutions can be briefly summarized if appropriate sources are cited; however, new components that have been modified or adapted should be described in detail. Furthermore, sustainable analyses and data evaluation approaches should be described, including the benefits of the results and the presentation of the results.

A. Reference Antenna Design

The first step of the process includes designing reference antennas that will operate at ZigBee 868 MHz and WiMAX 3500 MHz frequencies in a simulation environment. Using CST Microwave Studio (Computer Simulation Technology, 2016), antennas targeting ZigBee and WiMAX frequency bands have been modeled. Reference antennas consist of structures with traditional microstrip patch antenna geometry. Three distinct dielectric substrates, FR4, RO3203, and RT6006, selected for the proposed antenna designs, with relative permittivities of 4.3, 3.02, and 6.45, respectively. These materials are widely employed in microstrip antenna applications due to their favorable electromagnetic properties and robustness against environmental factors such as temperature variations and humidity which is an important issue when considering that antennas in smart grids will also operate in outdoor environments (Rogers Corporation, 2017; Laminated Plastics Corporation, 2017). In this context, employing substrates with varying dielectric constants enables a clearer evaluation of the influence of the proposed antenna model across different materials. The thicknesses of the selected dielectric substrates correspond to practical, commercially available values: 1.5 mm for FR4, 0.75 mm for RO3203, and 1.9 mm for RT6006. The design process of the rectangular patch antenna was carried out based on the transmission line model, utilizing Eq. 1 – Eq. 4 to determine the fundamental parameters (Balanis, 2005).

$$W_{patch} = \frac{c}{2f_r}\sqrt{\frac{2}{\varepsilon_r + 1}} \tag{1}$$

$$\varepsilon_{reff} = \frac{\varepsilon_r + 1}{2} + \frac{\varepsilon_r - 1}{2}\left[1 + 12\frac{h}{W_{patch}}\right]^{-\frac{1}{2}} \tag{2}$$

$$\frac{\Delta L_{patch}}{h} = 0.412\frac{\left(\varepsilon_{reff} + 0.3\right)\left(\frac{W_{patch}}{h} + 0.264\right)}{\left(\varepsilon_{reff} - 0.258\right)\left(\frac{W_{patch}}{h} + 0.8\right)} \tag{3}$$

$$L_{patch} = \frac{c}{2f_r\sqrt{\varepsilon_{reff}}} - 2\Delta L_{patch} \tag{4}$$

In the aforementioned equations, c denotes the speed of light in free space, f_r represents the resonant frequency of the antenna and ε_r refers to the relative permittivity (dielectric constant) of the substrate material. According to these parameters, the antenna width, W_{patch}, is calculated with Eq. 1. Then, effective dielectric constant, ε_{eff}, due to scattering is determined according to Eq. 2. After the amount of elongation due to scattering ΔL is calculated according to Eq. 3, finally the length of the patch antenna, L_{patch}, is obtained with the help of Eq. 4. The reference antenna model, depicted in Figure 1, is characterized by several key design parameters: the patch width (W_{patch}) and length (L_{patch}), the inset feed length (F_i) and width (g), and the microstrip feed line width (W_{feed}) and length (L_{feed}). The feed line parameters were calculated to comply with a 50Ω input impedance. Additionally, the substrate's dimensions are defined by its width (W_{subs}) and length (L_{subs}). While there is no definitive method for determining dielectric substrate size, the dimensions in this study

were optimized based on the rule that the distance between the ground plane edges and the patch edges should be no less than a quarter wavelength (Huang, 1983). The specific design parameters for each antenna are presented in Tables 1-6.

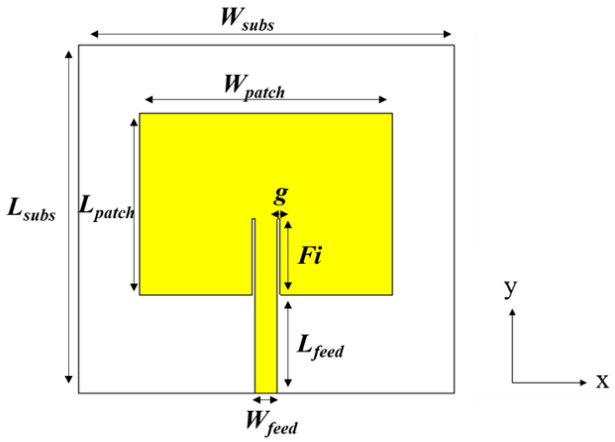


Figure 1. Reference patch antenna design.

Table 1. Reference antenna parameters for FR4 material at 868 MHz ZigBee band (mm).

W_{patch}	L_{patch}	W_{subs}	L_{subs}	g
104.16	81.60	187.18	146.55	0.55
F_i	W_{feed}	L_{feed}	t	h
32.96	3	23.45	0.035	1.524

Table 2. Reference antenna parameters for RO3203 material at 868 MHz ZigBee band (mm).

W_{patch}	L_{patch}	W_{subs}	L_{subs}	g
121.11	98.65	220.50	175.41	0.65
F_i	W_{feed}	L_{feed}	t	h
33.85	3	27.06	0.035	0.75

Table 3. Reference antenna parameters for RT6006 material at 868 MHz ZigBee band (mm).

W_{patch}	L_{patch}	W_{subs}	L_{subs}	g
88.81	67.39	157.90	121.80	0.45
F_i	W_{feed}	L_{feed}	t	h
31.99	3	19.87	0.035	1.9

Table 4. Reference antenna parameters for FR4 material at 3500 MHz WiMAX band (mm).

W_{patch}	L_{patch}	W_{subs}	L_{subs}	g
26.06	20.02	47.46	36.57	0.14
F_i	W_{feed}	L_{feed}	t	h
8.20	3	5.86	0.035	1.50

Table 5. Reference antenna parameters for RO3203 material at 3500 MHz WiMAX band (mm).

W_{patch}	L_{patch}	W_{subs}	L_{subs}	g
30.21	24.43	55.37	43.76	0.17
F_i	W_{feed}	L_{feed}	t	h
9.92	3	6.75	0.035	0.75

Table 6. Reference antenna parameters for RT6006 material at 3500 MHz WiMAX band (mm).

W_{patch}	L_{patch}	W_{subs}	L_{subs}	g
22.19	16.38	40.23	30.36	0.12
F_i	W_{feed}	L_{feed}	t	h
7.71	3	4.96	0.035	1.9

B. Proposed Antenna Design

The design progression of the proposed antenna, engineered for operation at 868 MHz (ZigBee) and 3500 MHz (WiMAX), is presented in Figure 2. The stages of this progression include the reference antenna, designated as 'Antenna #1', and the proposed antenna model, designated as 'Antenna #2'. To achieve bandwidth enhancement, two rectangular slots are etched into the patch. These slots are positioned symmetrically along the -y-axis, extending from the center of the upper patch edge toward the feed line. The dimensions of the slots are defined by their respective widths (a_1, a_2) and lengths (b_1, b_2).

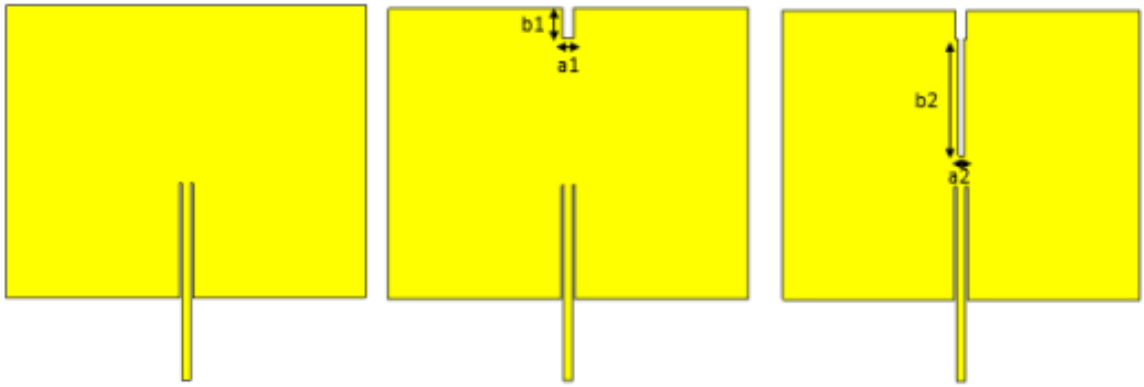


Figure 2. Proposed antenna design stages for FR4, RO3203, RT6006 materials, (a) Reference antenna design, Antenna#1 (b) Antenna design with one rectangular slot, (c) New model antenna design, Antenna#2.

Since three different dielectric materials are considered for two distinct frequency bands, the operating wavelength λ of each antenna varies depending on the substrate properties and target frequency. In order to establish a standardized and transferable design procedure, the slot dimensions were therefore defined as normalized fractions of the operating wavelength. Based on the simulation results, setting the first rectangular slot dimensions to approximately $a_1 \approx \lambda/50$ in width and $b_1 \approx \lambda/20$ in length was found to be optimal for bandwidth enhancement. These dimensions introduce a controlled capacitive loading and effectively extend the surface current path on the patch without significantly disturbing the fundamental resonant mode. As a result, closely spaced resonant modes are excited, and their overlap leads to an increased impedance bandwidth. To further enhance this effect, the dimensions of the second rectangular slot were defined relative to the first one as $a_2 = a_1/2$ and $b_2 = 4 \times b_1$, which provided an additional improvement in bandwidth. Because all slot dimensions are expressed as wavelength-scaled parameters, the same bandwidth enhancement mechanism remains valid across different dielectric materials and frequency bands, enabling a material-independent and frequency-scalable antenna design methodology. A detailed quantitative analysis of these effects is presented in the following section.

III. RESULTS AND DISCUSSIONS

The resonance frequency operations of the reference antennas and the newly designed structures have been analyzed through simulations. Thanks to introducing rectangular slots from the upper edge of the patch in the -y direction increased bandwidth or reduced return loss levels have been obtained. The width and length of the rectangular slots are related to the operating wavelengths of the antennas. Thus, the same design procedure is applicable to each antenna. The frequency responses of the reference antennas designed with FR4, RO3203, and RT6006 materials are shown in the plots below.

A. Simulation Results of Frequency Responses for The Antennas

Figure 3a shows the frequency response graphs of Antenna #1 and Antenna #2, both designed for ZigBee 868 MHz using FR4 material. Antenna #1 exhibits a return loss of -58.013 dB at 868 MHz, with a bandwidth of 7.26 MHz. Antenna #2 resonates at 869 MHz with a return loss of -46 dB and a bandwidth of 7.39 MHz. For the antenna model proposed with FR4 material, only a 0.13 MHz increase in bandwidth was achieved.

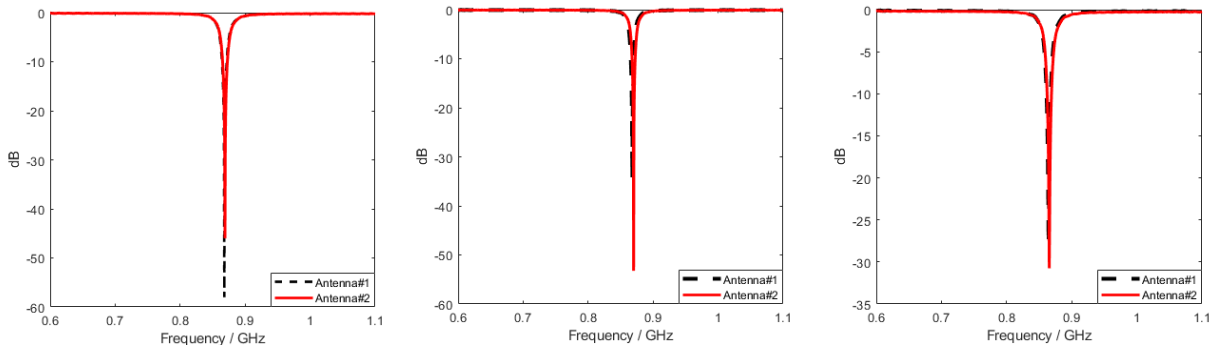


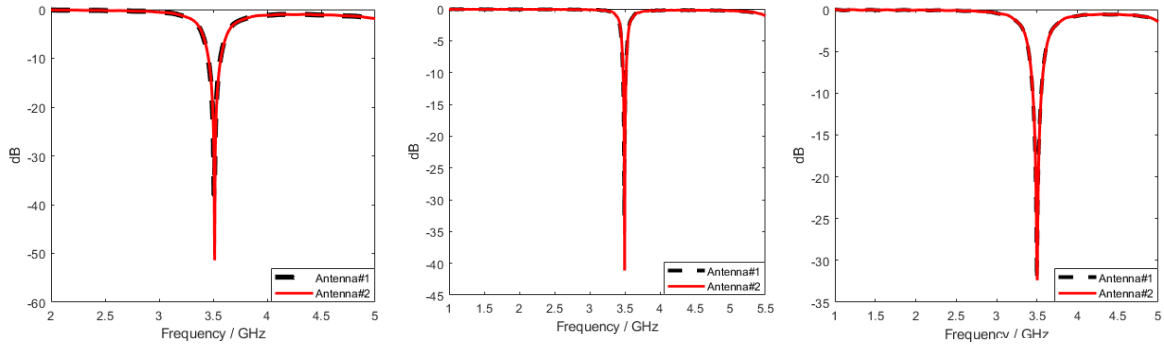
Figure 3. S11 parameters vs frequency response plot of ZigBee 868 MHz Antenna#1 and Antenna#2 with a) FR4, b) RO3203, c) RT6006.

Figure 3b shows the frequency response graphs of Antenna #1 and Antenna #2, both designed for ZigBee 868 MHz using RO3203 material. Antenna #1 has S11 levels of -34.66 dB at the target frequency of 868 MHz, with a bandwidth of 4.67 MHz. Antenna #2 resonates at 870 MHz with S11 levels of -53.23 dB and a bandwidth of 4.81 MHz. In the antenna designed with RO3203 material, the bandwidth increased by 0.14 MHz, and S11 level improved by 18.57 dB.

Figure 3c shows the frequency response plots of Antenna #1 and Antenna #2, both designed for ZigBee 868 MHz using RT6006 material. Antenna #1 has S11 levels of -28.01 dB at a frequency of 864.5 MHz, with a bandwidth of 6.51 MHz. Antenna #2 resonates at 865.5 MHz with S11 levels of -30.74 dB and a bandwidth of 6.71 MHz. In the antenna designed with RT6006 material, the bandwidth increased by 0.20 MHz, and S11 levels improved by 2.73 dB.

Antennas for the WiMAX 3500 MHz frequency were also designed using the same design procedure. The following figures present the results. Figure 4a shows frequency response graphs of Antenna #1 and Antenna #2, both designed for WiMAX 3500 MHz using FR4 material. Antenna #1 has S11 levels of -37.97 dB at 3508.5 MHz, with a bandwidth of 114.62 MHz. Antenna #2 resonates at 3514 MHz with S11 levels of -51.41 dB and a bandwidth of 115.29 MHz. In the antenna designed with FR4 material, the bandwidth increased by 0.67 MHz, and S11 levels improved by 13.44 dB.

Figure 4b shows the frequency response graphs of Antenna #1 and Antenna #2, both designed for WiMAX 3500 MHz using RO3203 material. Antenna #1 has S11 levels of -32.69 dB at 3492 MHz, with a bandwidth of 43.70 MHz. Antenna #2 resonates at 3497.5 MHz with S11 levels of -41.13 dB and a bandwidth of 43.85 MHz. In the antenna designed with RO3203 material, the bandwidth increased by 0.15 MHz, and S11 levels improved by 8.44 dB. Figure 4c shows the frequency response graphs of Antenna #1 and Antenna #2, both designed for WiMAX 3500 MHz using RT6006 material. Antenna #1 has S11 levels of -32.37 dB at 3497.5 MHz, with a bandwidth of 105.49 MHz. Antenna #2 resonates at 3503 MHz with S11 levels of -32.56 dB and a bandwidth of 106.56 MHz. In the antenna designed with RT6006 material, only a 1.07 MHz increase in bandwidth was observed.



(a) (b) (c)

Figure 4. S11 parameters vs frequency response plot of WiMAX 3500 MHz Antenna#1 and Antenna#2 with a) FR4, b) RO3203, c) RT6006.

B. Parametric Analyses Results

Parametric analyses conducted for different dimensions of rectangular slots in antenna models designed for the 868 MHz ZigBee and 3500 MHz WiMAX bands, using various substrate materials, are summarized in Tables 7–12. The tables show how changes in the resonant frequency and return loss levels occur when the short edges (a1 and a2 parameters) and long edges (b1 and b2 parameters) of the rectangular slots, introduced along the -y axis from the upper edge of the patch, are varied.

Table 7. Parametric analysis results of Antenna#2 in the ZigBee band for the FR4 material.

FR4						
	a1 (mm)			**a2 (mm)**		
	2.25	3.25	4.25	0.4	1.4	2.4
fr (MHz)	869	869	869.5	869	869	869.5
S11 (dB)	-37.5	-46	-35.5	-47.25	-46	-33.32

	b1 (mm)			**b2 (mm)**		
	6.2	8.2	10.2	30	32	34
fr (MHz)	869	869	868.5	869	869	869
S11 (dB)	-46.44	-46	-37.55	-33.93	-46	-37.18

Table 8. Parametric analysis results of Antenna#2 in the WiMAX band for the FR4 material.

FR4						
	a1 (mm)			**a2 (mm)**		
	0.78	0.82	0.86	0.22	0.44	0.66
fr (MHz)	3514	3514	3514	3514	3514	3514
S11 (dB)	-48.04	-51.41	-53.77	-48.21	-51.41	-46.89

	b1 (mm)			b2 (mm)		
	1.06	2.06	3.06	4.2	8.2	12.2
fr (MHz)	3514	3514	3514	3514	3514	3514
S11 (dB)	-46.98	-51.41	-47.38	-53.71	-51.41	-46.39

Tables 7 and 8 show the results of the parametric analyses in the ZigBee and WiMAX bands, respectively, for the FR4 material. For FR4, variations in the slot edge dimensions did not cause significant changes in the resonant frequencies of the antennas in either frequency band. However, more substantial variations in return loss levels were observed in the

ZigBee band, while changes in the WiMAX band occurred within a narrower range. For example, return loss levels in the ZigBee band varied between -33.32 dB and -47.25 dB, whereas in the WiMAX band, they ranged from -46.39 dB to -53.77 dB.

Table 9. Parametric analysis results of Antenna#2 in the ZigBee band for the RO3203 material.

RO3203						
	a1 (mm)			**a2 (mm)**		
	2.9	3.9	4.9	0.9	1.9	2.9
fr (MHz)	869	870	870.5	870	870	870
S11 (dB)	-29.57	-53.23	-34.45	-39.18	-53.23	-30.49

	b1 (mm)			**b2 (mm)**		
	8	10	12	35	37	39
fr (MHz)	870	870	870.5	870	870	870
S11 (dB)	-53.23	-53.23	-29.68	-37.74	-53.23	-41.57

Table 10. Parametric analysis results of Antenna#2 in the WiMAX band for the RO3203 material.

RO3203						
	a1 (mm)			**a2 (mm)**		
	0.586	0.986	1.386	0.293	0.493	0.693
fr (MHz)	3497.5	3497.5	3503	3497.5	3497.5	3497.5
S11 (dB)	-28.95	-41.13	-28.72	-37.71	-41.13	-43.32

	b1 (mm)			**b2 (mm)**		
	1.465	2.465	3.465	8.9	10.9	12.9
fr (MHz)	3497.5	3497.5	3497.5	3497.5	3497.5	3497.5
S11 (dB)	-38.65	-41.13	-41.61	-36.51	-41.13	-41.18

Tables 9 and 10 present the parametric analysis results for the RO3203 material in the ZigBee and WiMAX bands, respectively. Variations in the slot edge dimensions for the RO3203 material did not lead to significant changes in the resonant frequencies of the antennas in either frequency band.

Regarding return loss levels, similar to the results observed with FR4, greater variations were seen in the ZigBee band, while changes in the WiMAX band occurred within a narrower range. For instance, return loss levels in the ZigBee band ranged approximately from -29.57 dB to -53.23 dB, whereas in the WiMAX band, they were observed between -28.72 dB and -43.32 dB.

Table 11. Parametric analysis results of Antenna#2 in the ZigBee band for the RT6006 material.

RT6006						
	a1 (mm)			**a2 (mm)**		
	1.5	2.5	3.5	0.25	1.25	2.25
fr (MHz)	864.5	865.5	866.5	866	865.5	865.5
S11 (dB)	-27.35	-30.74	-25.13	-29.46	-30.74	-27.75

	b1 (mm)			**b2 (mm)**		
	4.8	6.8	8.8	25.4	27.4	29.4
fr (MHz)	865.5	865.5	865	865.5	865.5	865.5
S11 (dB)	-31.53	-30.74	-28.87	-29.28	-30.74	-30.05

Table 12. Parametric analysis results of Antenna#2 in the WiMAX band for the RT6006 material.

RT6006						
	a1 (mm)			a2 (mm)		
	0.37	0.67	0.97	0.09	0.29	0.49
fr (MHz)	3497.5	3503	3503	3503	3503	3503
S11 (dB)	-32.38	-32.37	-34.28	-32.13	-32.37	-32.19

	b1 (mm)			b2 (mm)		
	0.68	1.68	2.68	2.75	6.75	10.75
fr (MHz)	3503	3503	3503	3503	3503	3503
S11 (dB)	-32.74	-32.37	-32.48	-33.36	-32.37	-32.27

Tables 11 and 12 present the parametric analysis results for the RT6006 material in the ZigBee and WiMAX bands, respectively. For RT6006, variations in the slot edge dimensions did not cause significant changes in the resonant frequencies of the antennas in either frequency band. In terms of return loss levels, unlike the results for FR4 and RO3203, the variations were observed within narrow ranges. For example, return loss levels in the ZigBee band ranged approximately from -25.13 dB to -31.53 dB, while in the WiMAX band, they varied between -32.13 dB and -34.28 dB.

C. Far-Field Characteristics of The Proposed Antennas

This section presents the far-field characteristics of the proposed antennas, including radiation patterns, gain, and directivity. The simulations were carried out at the target operating frequencies, and the results are analyzed to evaluate the antennas' performance in terms of directional behavior and efficiency. The far-field radiation patterns of the antennas designed with FR4, RO3203, and RT6006 dielectric materials for the WiMAX and ZigBee bands are shown in Figure 5 and Figure 6, respectively. Overall, the main lobes of the designed antennas effectively direct or receive a significant portion of the radiated energy in the desired direction. Among them, the antenna using RO3203 material exhibited the lowest side lobe level at -15.7 dB and also delivered the highest power in the 5° main lobe direction. The antenna with FR4 material had the lowest radiation power in the main lobe direction at 2.33 dB, while the RT6006-based antenna reached 3.17 dB in the same direction.

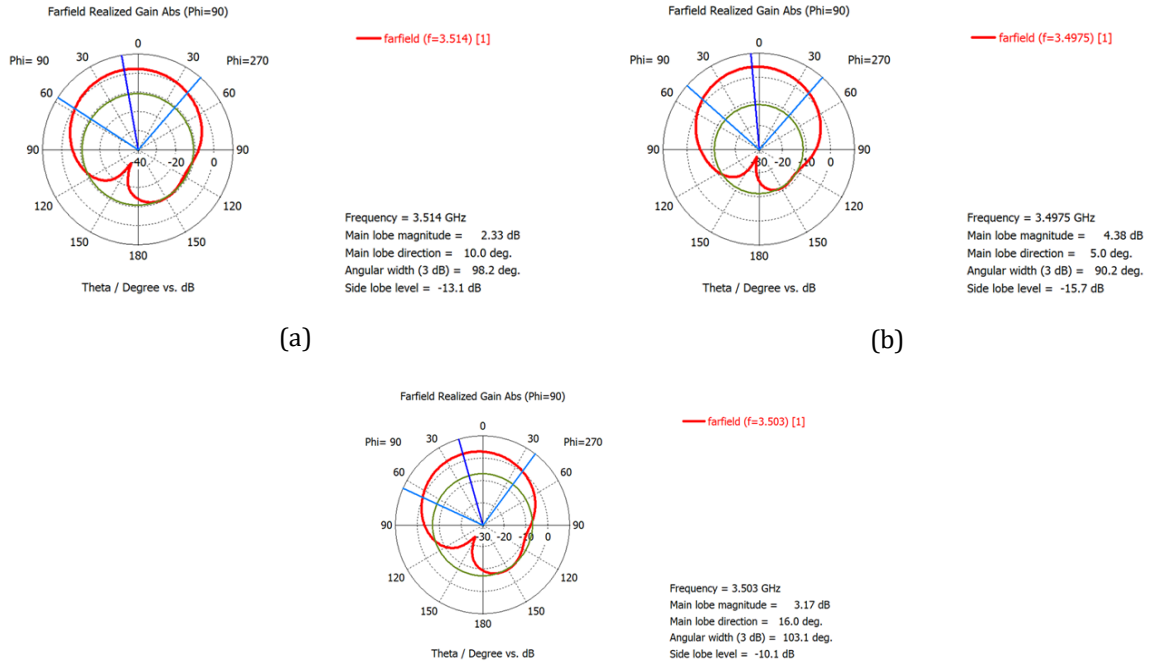


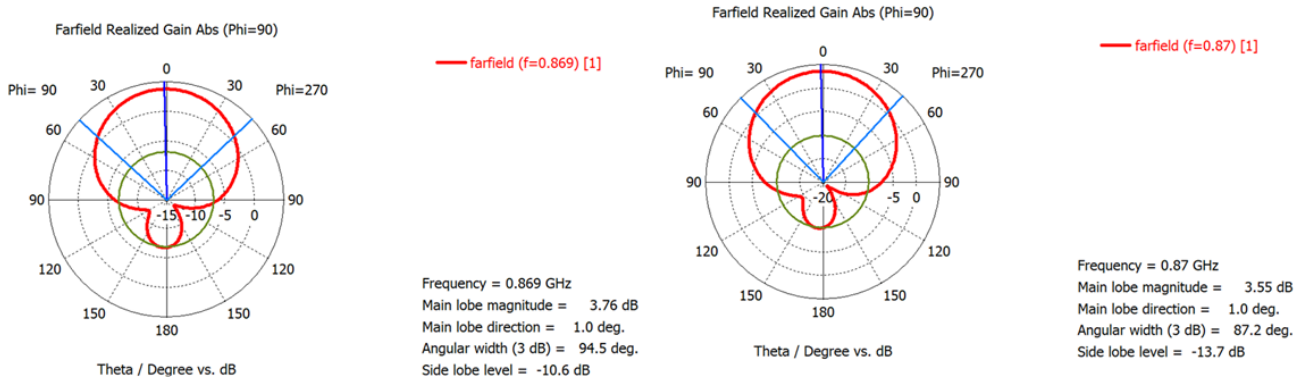
Figure 5. Far-field radiation pattern of Antenna #2 designed for WiMAX 3500 MHz band using, a) FR4, b) RO3203, c) RT6006.

The antenna simulation results provide key parameters such as main lobe intensity, main lobe angle, 3 dB beam width, and side lobe levels at the resonant frequencies of the designed antennas. These characteristic values for the antennas designed for data transmission in the WiMAX bands are summarized in Table 13 below.

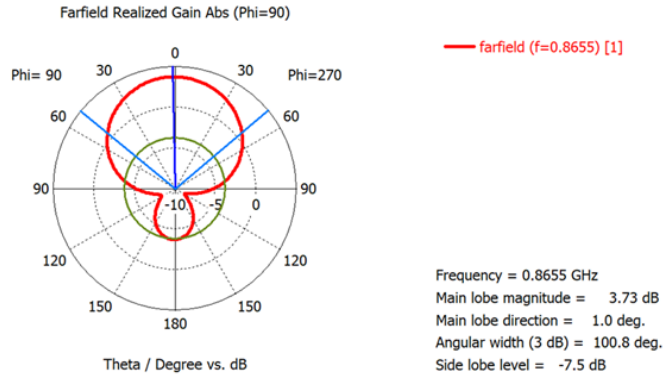
Table 13. Far-field characteristics of the proposed antennas for the WiMAX band.

	FR4	**RT6006**	**RO3203**
Frequency (GHz)	3.514	3.503	3.4975
Main Lobe Magnitude (dB)	2.33	3.17	4.38
Main Lobe Direction (deg)	10	16	5
3 dB Angular Width (deg)	98.2	103.1	90.2
Side Lobe Level (dB)	-13.1	-10.1	-15.7

Figure 6a, 6b and 6c show the far-field radiation patterns of antennas designed for the ZigBee band using FR4, RT6006, and RO3203 materials, respectively.



(a) (b)



(c)

Figure 6. Far-field radiation pattern of Antenna #2 designed for ZigBee 868 MHz using, a) FR4, b) RO3203, c) RT6006.

Using the same design procedure, antennas designed for the ZigBee 868 MHz band exhibited more stable performance than those designed for the WiMAX band. The main lobe direction was consistently at 1° for antennas fabricated with FR4, RT6006, and RO3203 materials. The main lobe intensities were similar across the three materials, measuring 3.76 dB, 3.73 dB, and 3.55 dB for FR4, RT6006, and RO3203, respectively. Among the antennas, the RO3203 design had the lowest side lobe level, while the FR4 antenna exhibited the highest.

The far-field characteristics are summarized in Table 14. Overall, the radiation patterns indicate that antennas designed for the ZigBee band concentrate more power in a specific direction compared to those designed for the WiMAX band.

Table 14. Far-field chracteristics of the proposed antennas for the ZigBee band.

	FR4	**RT6006**	**RO3203**
Frequency (GHz)	0.869	0.8655	0.87
Main Lobe Magnitude (dB)	3.76	3.73	3.55
Main Lobe Direction (deg)	1	1	1
3 dB Angular Width (deg)	94.5	100.8	87.2
Side Lobe Level (dB)	-10.6	-7.5	-13.7

D. Fabrication and Measurement

Among the antennas designed and simulated in the software environment, the antenna using RO3203 dielectric material—selected for its compact size and suitability for the WiMAX band—was chosen for fabrication. It should be noted that experimental fabrication and measurement were performed only for the antenna designed with the RO3203 substrate. This choice was motivated by the favorable balance offered by RO3203 in terms of low dielectric loss, dimensional stability, and fabrication reliability at the WiMAX frequency band. Moreover, among the investigated substrates, RO3203 exhibited the most consistent overall performance in simulations, including impedance matching, gain, and radiation characteristics. Since the main objective of this study is to validate a wavelength-scaled and material-independent slot design methodology, simulation and measurement results obtained with RO3203 is considered sufficient to experimentally confirm the proposed design approach, while the comparative behavior of different substrates is thoroughly assessed through numerical analyses.

The antenna was manufactured using a printed circuit board (PCB) engraving machine and tested with a vector network analyzer (VNA). Two identical antennas were produced for the chosen material and frequency band, intended to function as the transmitter and receiver. Figure 7 shows photographs of these antennas. To evaluate their real-world performance, measurements were carried out using the VNA. The measurement results for the antennas fabricated with RO3203 material over the 2–5 GHz frequency range are presented in Figure 8a and Figure 8b. Figure 8a shows the measurement result of the antenna in the left-hand side in Figure 7 presented by Measurement#1 and Figure 8b shows the measurement result of the antenna in the right-hand side in Figure 7 presented by Measurement#2.



Figure 7. Photos of the fabricated antennas with RO3203 substrate.

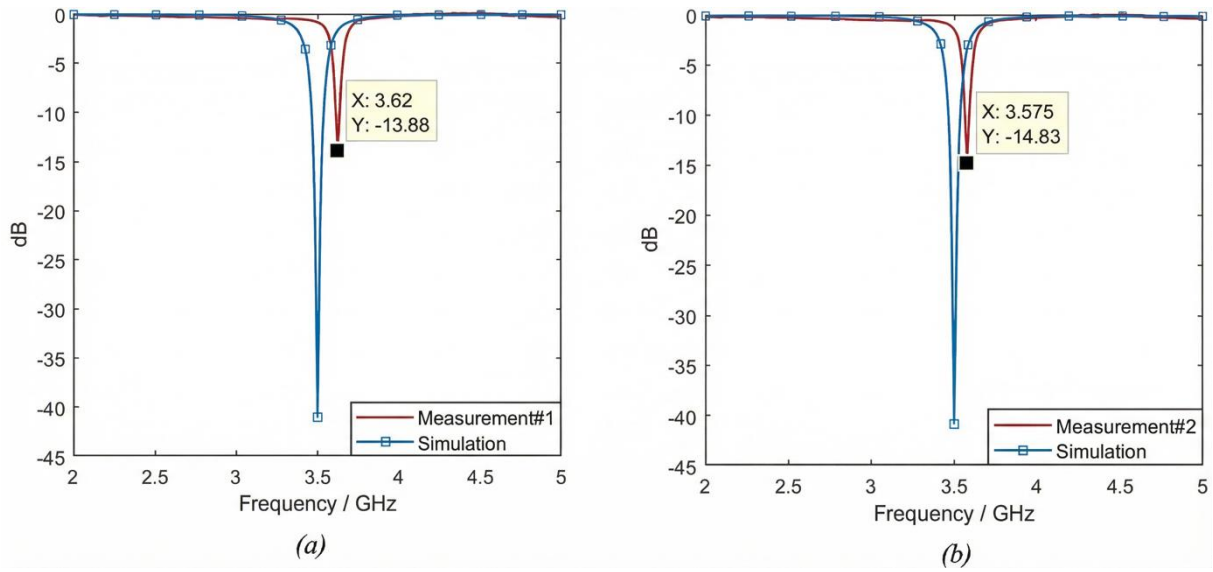


Figure 8. Comparison between the simulation and measurement results of the antennas with RO3203.

The simulation and measurement results of the antennas designed with RO3203 material and operating as a transmitter and receiver pair are compared in Figures 8a and 8b. The antenna based on the RO3203 substrate, which demonstrated the best performance in terms of gain and side lobe levels in the simulation results, also exhibited strong propagation characteristics in the measurements carried out after fabrication. The return loss level remains close to 0 dB at frequencies outside the resonance band, indicating minimal reception of unwanted signals. This behavior suggests that the antenna is largely insensitive to environmental interference when operating either as a transmitter or as a receiver. Such a characteristic is particularly important for ensuring reliable and stable data transmission in smart grid communication applications. The remaining discrepancies between the simulated and measured results can be attributed to fabrication tolerances, feeding and connector effects, and various loss mechanisms that influence antenna performance. In particular, limitations in copper etching accuracy and variations in feed-line geometry introduce deviations from the idealized simulation model. In addition, the measurement environment and setup play a significant role in the observed differences. Reflections from nearby objects, cables, and fixtures, as well as imperfect calibration of the VNA, can affect the measured return-loss response.

The application was made with antennas using materials. One of the antennas was connected to the signal generator to be used as a transmitter. The other was connected to the spectrum analyzer input. A 25 dBm amplitude signal at a frequency of 3.56 GHz was given to the antenna used as a transmitter. The antenna with the signal generator used is shown in Figure 9.

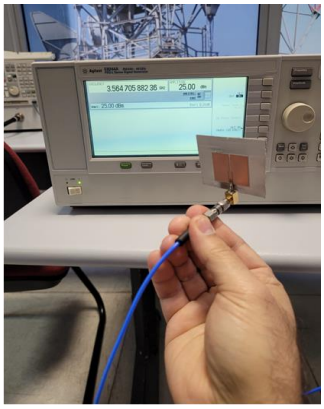


Figure 9. The signal applied to the antenna with RO3203 substrate used as the transmitter.

The antenna to be used as the receiver is connected to the input of the spectrum analyzer. As seen in Figure 10, it is seen on the spectrum analyzer's screen that there is a peak at 3.57 GHz which means the signal sent at exactly 3.57 GHz is received. In this way, the data on smart meters or sensor output information in smart networks can be transferred wirelessly to the desired center using the WiMAX frequency band. If desired, the antennas can be directly connected to the analog data outputs of smart meters or mounted on the ADC (Analog Digital Converter) output to transfer the converted data to digital.

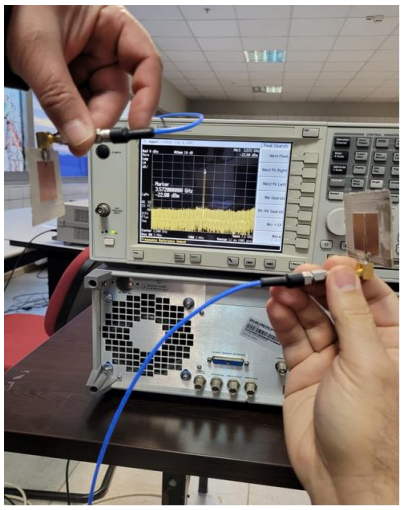


Figure 10. The application of the antennas with RO3203 used as a transmitter-receiver pair.

Although slotted microstrip patch antennas have been extensively investigated in the literature for various wireless applications, most existing studies focus on a single dielectric substrate and rely on empirically optimized slot geometries tailored to a specific frequency band or application (Regina et al., 2025; Paul et al., 2021; Shanmugasundaram et al., 2025). In contrast, the main novelty of this study lies in proposing a wavelength scaled, material independent slot design methodology that can be systematically applied across different dielectric substrates and frequency bands without reoptimization. The rectangular slot dimensions are explicitly defined as fixed fractions of the operating wavelength (e.g., $\lambda/50$ and $\lambda/20$), allowing the same design rules to be directly transferred to both ZigBee (868 MHz) and WiMAX (3.5 GHz) bands. Using this unified approach, a total of six antennas employing three widely used substrates, namely (a) FR4, (b) RO3203, and (c) RT6006, across two frequency bands are designed, simulated, fabricated, and experimentally validated. Unlike prior works that primarily emphasize multiband behavior, complex slot geometries, or single material performance (Krishna et al., 2023; Jadhav et al., 2023; Paul et al., 2021), the proposed study provides a comparative, multimaterial performance assessment relevant to heterogeneous smart grid deployment environments. To clearly highlight these distinctions, Table 15 presents a systematic comparison between the proposed work and recent literature by jointly considering slot design rules, number of substrates, application focus, radiation characteristics, and measured performance, while explicitly including the features of the present study for direct comparison.

Table 15. Comparison of the proposed work with recent slotted microstrip patch antenna studies.

Ref.	**Frequency Band(s)**	**Substrate(s)**	**Slot Design Strategy**	**Multi-Material Analysis**	**Fabrication & Measurement**	**Main Contribution**
Regina et al. (2025)	3–3.3 GHz (IoT)	FR4	Empirical slot optimization	No	Simulation only	Shape-optimized slotted antenna for IoT
Krishna et al. (2023)	S-band	Single custom substrate	Fixed rectangular slots	No	Simulation only	Dual-slot antenna for S-band
Jadhav et al. (2023)	Multi-band	FR4	Geometry-based slotting	No	Simulation only	Multiband circular patch antenna
Paul et al. (2021)	WiFi / ZigBee	FR4	Partial ground & slots	No	Fabrication	Compact multiband antenna
Paul et al. (2022)	5G / WiFi / WiMAX	RT5880	Π-shaped slots	No	Fabrication	Wideband slotted patch design
Shanmugasundaram et al. (2025)	WiFi / ZigBee / WiMAX	FR4	Empirical slot geometry	No	Fabrication	Multiband slotted antenna for wireless systems
This work	ZigBee (868 MHz), WiMAX (3.5 GHz)	(a) FR4, (b) RO3203, (c) RT6006	Wavelength-scaled, rule-based slot design	Yes (3 substrates)	Yes (simulation + measurement)	Material-independent design methodology and comparative substrate evaluation for smart-grid communication

From Table 16, it is observed that most existing studies report either moderate directivity (typically below 3 dBi) or limited impedance matching, with return loss values generally ranging between −21 dB and −42 dB. In some studies, particularly (Regina et al., 2025), relatively high directivity is achieved; however, very deep return loss levels are not obtained, indicating a trade-off between radiation performance and matching quality.

In contrast, the proposed design demonstrates consistently strong performance in both metrics across multiple substrates and frequency bands. In particular, the return loss values of the proposed antenna significantly exceed those of prior studies, reaching levels below −50 dB, which indicates excellent impedance matching.

Table 16. Comparison of directivity and return loss with existing studies.

Ref.	Directivity (dBi)	Return Loss (dB)
Regina et al. (2025)	6.8	−25
Krishna et al. (2023)	−1.16	−21.6
Jadhav et al. (2023)	–	−34.54
Paul et al. (2021)	2.87	−42.17
Paul et al. (2022)	3.005	−36.81
Shanmugasundaram et al. (2025)	−3.77	−38.96
Proposed (FR4)	WiMAX: 2.33 ZigBee: 3.76	WiMAX: −51.41 ZigBee: −46.00
Proposed (RO3203)	WiMAX: 4.38 ZigBee: 3.55	WiMAX: −41.13 ZigBee: −53.23
Proposed (RT6006)	WiMAX: 3.17 ZigBee: 3.73	WiMAX: −32.37 ZigBee: −30.74

E. Contribution for Smart Grid Communication and Gain Calculation

The proposed antenna structures and design procedures in this work present important contributions to smart grid communication systems. Particularly, the utilization of various dielectric materials and the implementation of a unified methodology for each material result in a well-defined and systematic workflow while maintaining low return loss. Among the communication techniques that have been proposed for smart grid applications, narrowband IoT (NB-IoT) and narrowband PLC (Power Line Communication) are primary ones. Thus, for most of the smart grid communications, data rates of 10–500 kbps are adequate (Hasan et al., 2023). Therefore, the antennas proposed in this work are also well-suited for narrowband smart grid communication scenarios. The gain calculations were carried out using the simulation software. The default time-domain solver employs the Finite Integration Technique (FIT) (Dassault Systèmes, n.d.). In addition, a gain determination method has been proposed and validated using two log-periodic antennas (Mistry et al., 2019). The antenna models proposed in this paper exhibit good gain performance at their operating frequencies. Specifically, the antenna designed for the WiMAX frequency band using the RO3203 substrate achieves the highest gain of 4.38 dB, while the antennas designed with RT6006 and FR4 exhibit gains of 3.17 dB and 2.33 dB, respectively. For the antennas designed for the ZigBee frequency range, the gain values are 3.55 dB, 3.73 dB, and 3.76 dB for the RO3203, RT6006, and FR4 substrates, respectively. Figure 11 and Figure 12 show 3D far-field plot of the antennas for WiMAX and ZigBee bands, respectively, at their operating frequencies.

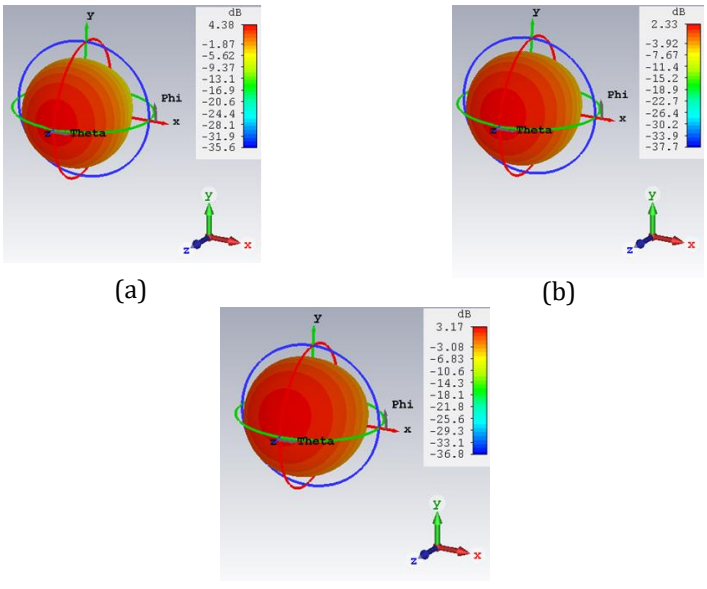
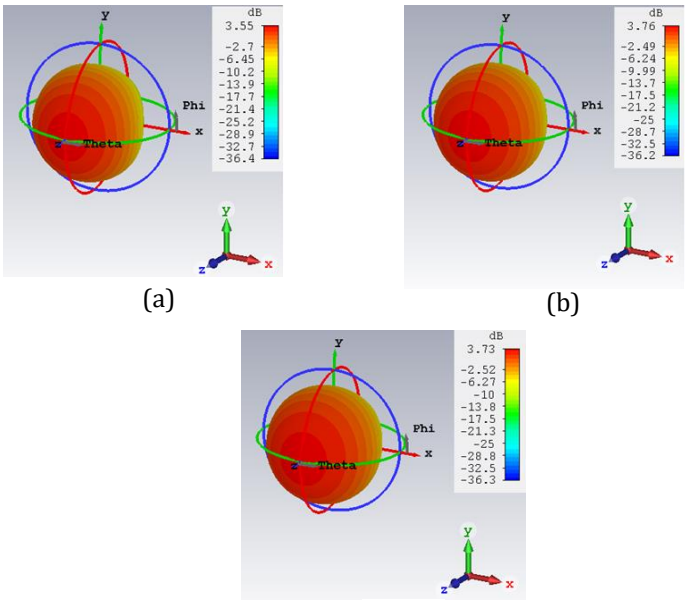


Figure 11. 3D Far-field plots of the antennas for WiMAX with the substrates of a) RO3203, b) FR4, c) RT6006.

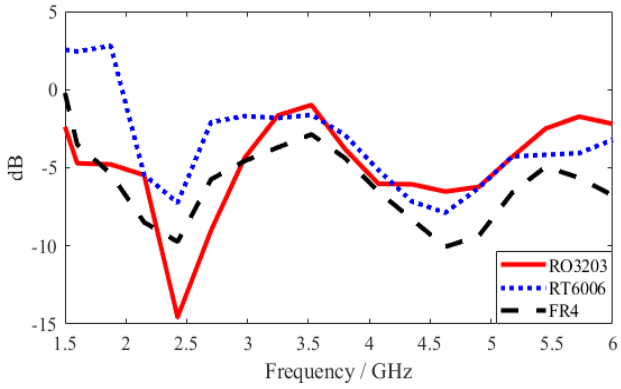


(a) (b)

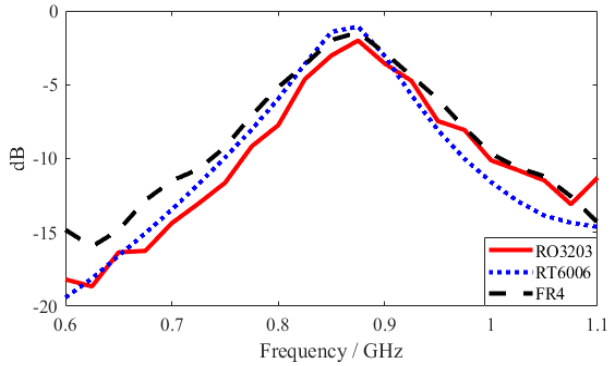
(c)

Figure 12. 3D Far-field plots of the antennas for ZigBee with the substrates of a) RO3203, b) FR4, c) RT6006.

Figure 13a and 13b present the broadband gain plots of the antennas for the WiMAX and ZigBee frequency ranges, respectively. As can be seen from the plot, an improvement in the gain characteristics is observed around the 3.5 GHz resonance region for the antennas designed with all three substrate materials. The antennas fabricated using RO3203 and RT6006 exhibit comparable performance within this band, both achieving relatively higher gain levels. In contrast, the FR4-based antenna demonstrates lower gain in the same frequency region. In a similar manner, an improvement in the gain characteristics is also observed around the resonance frequency for the ZigBee band. In this region, the antennas designed using RT6006 and FR4 dielectric substrates exhibit the highest performance, whereas the antenna designed with RO3203 shows a slightly lower gain level.



(a)



(b)

Figure 13. Gain vs Frequency plot of the proposed antennas a) WiMAX band, b) ZigBee band.

IV. CONCLUSION

This paper proposes new slotted microstrip patch antenna models for smart grid data transmission operating in the WiMAX (3.5 GHz) and ZigBee (868 MHz) frequency bands. The proposed design is based on etching rectangular slots along the −y direction from the upper edge of the patch and applying a unified, wavelength-scaled slot design procedure across different dielectric materials. Using this methodology, a total of six antennas were designed and analyzed by considering three widely used substrates, namely FR4, RO3203, and RT6006, for two different frequency bands.

The slot dimensions were optimized as fixed fractions of the operating wavelength to enhance the impedance bandwidth and radiation performance while preserving the fundamental resonant behavior. Simulation results demonstrate that, for the WiMAX band, the proposed antennas achieved broadband gain values ranging from 2.33 dB to 4.38 dB, whereas for the ZigBee band, the gain values varied between 3.55 dB and 3.76 dB, depending on the substrate material. In addition, significant improvements in return loss characteristics were observed, confirming the effectiveness of the proposed slot configuration. Among the investigated substrates, RO3203 exhibited the most favorable overall performance in terms of gain and side-lobe suppression, and therefore was selected for fabrication and experimental validation.

The fabricated RO3203-based antenna showed good agreement between simulated and measured S_{11} results, validating the proposed design methodology and confirming its practical feasibility. These results indicate that the proposed antenna structures are well suited for reliable wireless data transmission in smart grid communication scenarios, where compact size, stable radiation characteristics, and material flexibility are essential for heterogeneous deployment environments.

From a practical perspective, the proposed wavelength-scaled and material-independent design approach provides a transferable reference for antenna designers targeting smart grid, IoT, and low-power wireless communication systems operating in different frequency bands and substrate conditions. As future work, experimental validation of radiation patterns and gain measurements in an anechoic chamber will be conducted to further corroborate the simulated far-field results. In addition, extending the proposed methodology to multiband or reconfigurable antenna structures and investigating real-time smart grid deployment scenarios constitute promising directions for further research.

DECLARATIONS

Acknowledgements: This work was supported by Scientific Research Projects Coordination Unit of Bandırma Onyedi Eylül University. Project Number: BAP-23-1004-009.

Author Contributions: For multi-author articles, the specific contributions of each author should be indicated using their initials, for example: Conceptualization, B.G.H. and M.G.; Methodology, B.G.H. and İ.B.K; Software, B.G.H..; Validation, B.G.H.; Formal Analysis, B.G.H.; Investigation, B.G.H. and M.G.; Resources, B.G.H. and S.K.; Data Curation, S.K; Writing—Original Draft, B.G.H. and M.G.; Writing—Review & Editing, B.G.H. and M.G.; Visualization, B.G.H. and M.G.; Supervision, B.G.H. and M.G.; Project administration, B.G.H. and İ.B.K; Funding acquisition, B.G.H. All authors have read and approved the final version of the manuscript.

Conflict of Interest: The authors declare no conflict of interest.

Supporting Institutions: This work was supported by Scientific Research Projects Coordination Unit of Bandırma Onyedi Eylül University.

Ethical Approval: This study does not involve human or animal participants. All procedures followed scientific and ethical principles, and all referenced studies are appropriately cited.

Plagiarism Statement: This article has been evaluated for plagiarism and no instances of plagiarism were detected.

Use of AI Tools: The authors would like to acknowledge the use of an AI-based language assistance tool (ChatGPT, OpenAI) for improving the clarity, grammar, and readability of the manuscript. The tool was used exclusively for language refinement; all scientific content, methodology, results, and interpretations are solely the responsibility of the authors.

REFERENCES

Abdul Salam, R., Ratyal, N. I., Ahmed, U., Aziz, I., Sajid, M., & Mahmood, A. (2024). An overview of recent wireless technologies for IoT-enabled smart grids. *Journal of Electrical and Computer Engineering, 2024*, Article 2568751. https://doi.org/10.1155/jece/2568751

Abrahamsen, F. E., Ai, Y., & Cheffena, M. (2021). Communication technologies for smart grid: A comprehensive survey. *Sensors, 21*(23), Article 8087. https://doi.org/10.3390/s21238087

Balanis, C. A. (2005). *Antenna theory: Analysis and design*. John Wiley & Sons.

Belu, R. (2013). *Smart Grid Fundamentals: Energy Generation, Transmission and Distribution*. CRC Press.

Colak, I., Bayindir, R., & Sagiroglu, S. (2020). The effects of the smart grid system on the national grids. In *Proceedings of the 2020 8th International Conference on Smart Grid (icSmartGrid)* (pp. 122–126). https://doi.org/10.1109/icSmartGrid49881.2020.9144891

Computer Simulation Technology. (2016). *CST Microwave Studio (Version 2016)* [Computer software].

Dassault Systèmes. (n.d.). *CST Studio Suite: Electromagnetic simulation software* [Computer software]. https://www.3ds.com/products/simulia/cst-studio-suite

Dokmetas, B., Arican, G. O., & Yilmaz, B. A. (2024). A folded pyramid-shaped microstrip antenna with improved bandwidth. In *Proceedings of the IEEE International Symposium on Antennas and Propagation and INC/USNC-URSI Radio Science Meeting* (pp. 1273–1274). IEEE.

Hasan, M. K., Habib, A. A., Islam, S., Balfaqih, M., Alfawaz, K. M., & Singh, D. (2023). Smart grid communication networks for electric vehicles empowering distributed energy generation: Constraints, challenges, and recommendations. *Energies, 16*(3), Article 1140. https://doi.org/10.3390/en16031140

Huang, J. (1983). The finite ground plane effect on the microstrip antenna radiation patterns. *IEEE Transactions on Antennas and Propagation, 31*(4), 649–653. https://doi.org/10.1109/TAP.1983.1143108

Jadhav, A., Biradar, N., Bhaldar, H., Mathpati, M., Wadekar, R., & Deshmukh, M. (2023). Multiband, circular microstrip patch antenna for wireless applications. *Wireless Personal Communications, 128*(1), 173–186. https://doi.org/10.1007/s11277-022-09948-9

Kabeyi, M. J. B., & Olanrewaju, O. A. (2023). Smart grid technologies and application in the sustainable energy transition: A review. *International Journal of Sustainable Energy, 42*(1), 685–758. https://doi.org/10.1080/14786451.2023.2222298

Kataray, T., Nitesh, B., Yarram, B., Sinha, S., Cuce, E., Shaik, S., Vigneshwaran, P., & Roy, A. (2023). Integration of smart grid with renewable energy sources: Opportunities and challenges – a comprehensive review. *Sustainable Energy Technologies and Assessments, 58,* Article 103363. https://doi.org/10.1016/j.seta.2023.103363

Kishore, N., & Senapati, A. (2022). 5G smart antenna for IoT application: A review. *International Journal of Communication Systems, 35*(13), Article e5241. https://doi.org/10.1002/dac.5241

Krishna, N. R. P. S., Shirisha, H., Hussain Isfahani, A. M., & Manisha, K. (2023). Design of dual rectangular slotted microstrip patch antenna for S-band. In *Proceedings of the 4th International Conference for Emerging Technology* (pp. 1-6). IEEE. https://doi.org/10.1109/INCET57972.2023.10170206

Laminated Plastics Corporation. (2017). *FR4 technical datasheet* [Technical datasheet].

Mistry, K. K., Lazaridis, P. I., Zaharis, Z. D., Akinsolu, M., Liu, B., & Loh, T. (2019). Accurate antenna gain estimation using the two-antenna method. In *Proceedings of the Antennas and Propagation Conference (APC)* (pp. 1–4). https://doi.org/10.1049/cp.2019.0717

Onay, M. Y., & Dokmetas, B. (2025). 3D printed microstrip antenna for symbiotic communication: Wifi backscatter and bit rate evolution for IoT. *Internet of Things, 32*, Article 101643. https://doi.org/10.1016/j.iot.2025.101643

Pandiyan, P., Saravanan, S., Kannadasan, R., Krishnaveni, S., Alsharif, M. H., & Kim, M. K. (2024). A comprehensive review of advancements in green IoT for smart grids: Paving the path to sustainability. *Energy Reports, 11*, 5504–5531. https://doi.org/10.1016/j.egyr.2024.05.021

Paul, L. C., Ankan, S. S. A., & Lee, W. S. (2021). A slotted patch array antenna with a partial ground plane for WiFi/Bluetooth/ZigBee applications. In *Proceedings of the IEEE Indian Conference on Antennas and Propagation (InCAP)* (pp. 560–563). IEEE. https://doi.org/10.1109/InCAP52216.2021.9726451

Paul, L. C., Jim, M. T. R., Rani, T., Ankan, S. S. A., Das, S. C., & Saha, H. K. (2022). A Π-shaped slotted patch antenna with a partial ground structure for lower 5G/WiFi/WiMAX applications. *Heliyon, 8*(10), Article e10934. https://doi.org/10.1016/j.heliyon.2022.e10934

Regina, S., Vasuki, S., Savita, S., Ramya, S., & Kanmani, M. (2025). Design and optimization of different shape slotted patch antenna for IoT applications. In *Proceedings of the International Conference on Recent Advances in Electrical, Electronics, Ubiquitous Communication, and Computational Intelligence (RAEEUCCI)*. IEEE. https://doi.org/10.1109/RAEEUCCI63961.2025.11048356

Rogers Corporation. (2017). *RT/duroid 5880 high frequency laminates datasheet* [Technical datasheet].

Sendin, A., Matanza, J., & Ferrús, R. (2021). *Smart grid telecommunications: Fundamentals and technologies in the 5G era.* John Wiley & Sons.

Shanmugasundaram, P. P., R. S, P. V., D, A. J., Banerjee, S., & Sharma, K. (2025). A multiband slotted patch antenna for wireless applications. In *Proceedings of the 1st International Conference on Radio Frequency Communication and Networks (RFCoN)*. IEEE. https://doi.org/10.1109/RFCoN62306.2025.11085196